Small-Animal and Endoscopic PET Detector Modules Based on Multichannel Digital Silicon Photomultipliers

Venialgo Araujo, E.; Sinha, S.; Gong, T.; Mandai, S.; Carimatto, A.; Brunner, S. E.; Schaart, D.R.; Charbon, E.

DOI
10.1109/NSSMIC.2016.8069504

Publication date
2017

Document Version
Final published version

Published in
2016 IEEE Nuclear Science Symposium, Medical Imaging Conference and Room-Temperature Semiconductor Detector Workshop, NSS/MIC/RTSD 2016

Small-Animal and Endoscopic PET Detector Modules Based on Multichannel Digital Silicon Photomultipliers

E.Venialgo, S. Sinha, T. Gong, S. Mandai, A. Carimatto, S. E. Brunner, D. R. Schaart, and E. Charbon

***Abstract*—In time-of-flight (TOF) positron emission tomography (PET), the coincidence resolving time (CRT) has a strong influence on the overall performance. Multichannel digital silicon photomultipliers (MD-SiPMs) are able to obtain several timestamps for gamma photon timemark estimation. Using this feature, the CRT is improved and the system robustness is significantly increased by utilizing multiple photoelectron timestamps. In addition, the PET instrumentation chain is simplified because of the intrinsic digitization and integrated functionality of the MD-SiPM.**

The main objective of this work is to demonstrate the possibility of building a complete highly-miniaturized PET detector module for endoscopic applications. In addition, we show that it's possible to operate simultaneously several MD-SiPM array chips in order to build a small-animal PET detector modules.

We present the implementation of two PET detector modules that are based on MD-SiPMs: a small animal and an endoscopic PET detector modules. The small animal PET detector module consists of 2×4 monolithic MD-SiPM array chips. In addition, this module includes a low-cost field programmable gate array (FPGA), a temperature controlling system and data transfer interfaces. The endoscopic PET detector module comprises a single monolithic array of 9×18 MD-SiPM and a small form-factor FPGA. In this module, a remarkable level of compactness is achieved. Eventually, a thermal characterization and a preliminary radiation measurement are presented.

I. Introduction

When detecting scintillation photons with a single-photon counting detector, the first photon detected usually does not provide the optimum time information [1]. Better estimation of the time-of-interaction can be achieved by utilizing the timing information carried by multiple scintillation photons [2], [3].

MD-SiPMs in combination with ultra-fast and ultra-bright scintillators therefore can significantly improve on timing resolution by obtaining a very large number of timestamps, one for each light photon associated with the shower of optical photons that are triggered by a gamma-photon scintillation. Using appropriate mathematical techniques, one can show that the overall time resolution of the gamma photon timemark nevertheless is bounded [4], [3].

E. Venialgo, S. Sinha, A. Carimatto, T. Gong, S. Mandai, and E. Charbon, are with the Applied Quantum Architectures department, Delft University of Technology, Delft, Netherlands (e-mails: e.venialgo@tudelft.nl and e.charbon@tudelft.nl)

Stefan E. Brunner, Dennis R. Schaart are with the Radiation Science & Technology department, Delft University of Technology, Delft, The Netherlands.

The research has received funding from the European Union Seventh Framework Program under Grant Agreement n°289355 (PicoSEC-MCNet).

In this work, we present two types of PET detector modules based on MD-SiPMs: a small animal and an edoscopic PET detector modules.

II. Endoscopic PET Detector Module

The core of the PET detector module is the MD-SiPM array chip [5], [6]. MD-SiPMs enable to timestamp photon events sharing one time-to-digital converter (TDC) for a set of 8 SPADs, thus obtaining up to 48 timestamps for each scintillation event in an area of $0.8\times0.8\mu\mathrm{m}^2$.

MD-SiPM array chips are wire-bonded to a chip-on-board PCB (see Fig. 1) containing two temperature sensors and two SMD board-to-board connectors mounted on the bottom layer of the same PCB. These two SMD (surface mount device) receptacles are used for connecting the chip-on-board PCBs onto a miniaturized FPGA board or a motherboard PCB (see Figs. 2 and 4).

The MD-SiPM arrays' main application is the endoscopic PET in the context of the EndoTOF-PET US project [7]. It is a compact highly-integrated PET detector module, which contains all the required circuitry for operation, in a compact volume of $13.5\times30.2\times15.8\ \mathrm{mm}^3$.

The chip-on-board PCB is connected through the SMD receptacles to a miniaturized low-power Microsemi FPGA board (see Figs. 2 and 3). The miniaturized FPGA board contains the required low drop-out (LDO) regulators to operate the MD-SiPM array in addition to low-voltage differential signal (LVDS) data lines to send the information to an high-speed acquisition board [8].

A highly miniaturized PET detector module suitable for endoscopic PET applications is an LYSO:Ce scintillator matrix of 9×16 pixels on top of the chip-on-board PCB (see Fig. 3).

III. Small Animal PET Detector Module

The small animal PET detector module is composed of 4×2 MD-SiPM arrays mounted on a highly-miniaturized chip-on-board PCB that is connected onto a motherboard (see Fig. 4) [9].

The Motherboard PCB contains all the ecosystem required to operate the 4×2 MD-SiPM arrays. As shown in the final implementation, a high scintillator density can be achieved. The PCBs were designed to reduce the dead space between dies at a reasonable manufacturing cost. This module allows to build two rings of detectors by placing them in a mirrored way, in order to keep a small dead space between scintillators.

978-1-5090-1642-6/16/$31.00 ©2016 IEEE

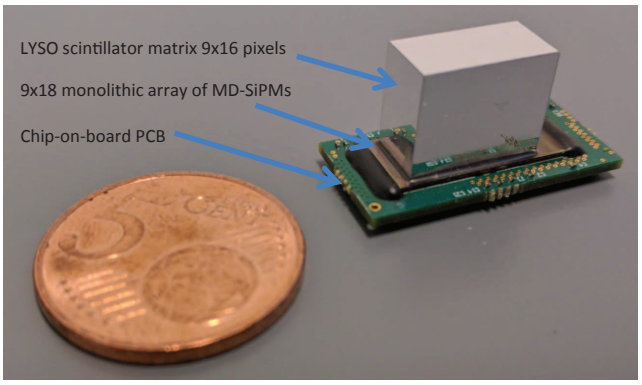

Fig. 1: Chip-on-board PCB with a wire-bonded MD-SiPM array and an LYSO:Ce array of 9×16 pixels glued on top.

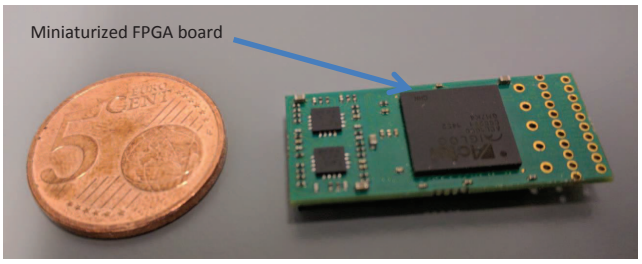

Fig. 2: Miniaturized Microsemi FPGA board.

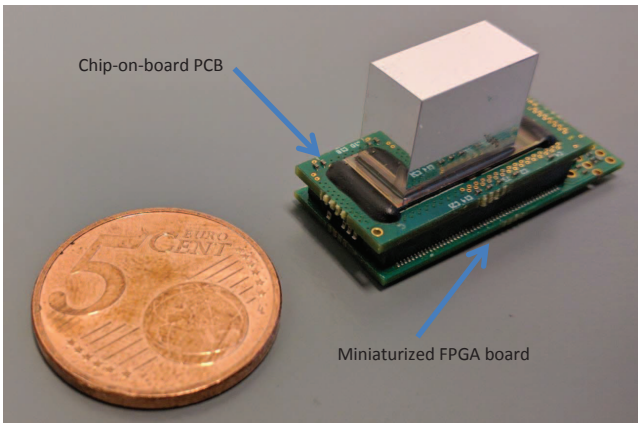

Fig. 3: Miniaturized Endoscopic PET Detector.

At this point of the design, all the power distribution networks (PDNs) were designed as independent as possible for testing purposes. Subsequently, there are 46 LDO regulators on board requiring extra space and reducing the scintillator packing fraction. An FPGA board (XCM-206Z-LX150) from HumanData Ltd. is plugged onto the back of the motherboard.

IV. PET Detector Module Characterization

A radiation characterization was performed utilizing a ^{22}Na radioactive source with an activity of 39.5 μCi. In this experiment we utilized two scintillator matrices, one of 4×9 LYSO:Ce pixels of 1.6 mm pitch, and a second matrix of 9×16 LYSO:Ce pixels of 0.8 mm pitch (see Fig.1). We operated the MD-SiPM array in a frame-based read out mode, which allows to access all SPAD cell data in every detection cycle. The source was placed about 1 cm away from the scintillator.

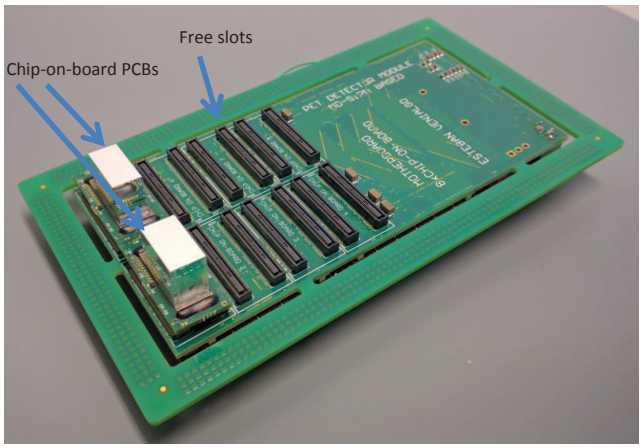

Fig. 4: Motherboard with two chip-on-board PCBs plugged. It has six more free slots (two connectors per slot).

Fig. 5a depicts a detected scintillation event from the 9×16 LYSO:Ce matrix that is measured and read out in frame-based mode. As observed, the SPAD cells that are triggered by scintillation photons can be clearly identified and they are surrounded by SPAD cells that are triggered by dark counts. As can be seen in the Fig. 5a, one complete MD-SiPM column and one complete MD-SiPM row were deactivated by using the SPAD cell masking circuitry.

Fig. 6a depicts the same measurement but when utilizing the chip-on-board PCB that has a 4×9 LYSO:Ce matrix with 1.6 mm pitch glued on top. As observed in the Fig. 6a, several MD-SiPM rows were deactivated during this measurement.

In addition, we performed a 9×16 LYSO:Ce matrix pixel-identification experiment. In this measurement, we activated all of the 9×18 MD-SiPMs except for the first column that was completely shut down. The center of a scintillation event was determined by post-processing the sensor's raw information (i.e., a boolean matrix indicating which SPAD detected a photon) and using a mass centroid algorithm.

Fig. 7 shows the 1-D histogram of the column coordinate of scintillation mass centroid. The scintillator matrix has 9×16 LYSO:Ce pixels but only data coming from 8 columns of pixels is detected because one column was completely shut down. Fig. 8 depicts the same 1-D histogram but row-wise. As observed, the 16 LYSO:Ce pixel rows can be identified. Fig. 9 shows the 2-D histogram of the coordinate of scintillation centroid of mass. The left LYSO:Ce pixel column is compressed towards the center of the map because of the deactivation of the first MD-SiPM column.

V. Cooling System

A cooling system for the small animal PET detector module was designed and manufactured by Dienst Elektronische en Mechanische Ontwikkeling (DEMO) at Delft University Technology. The cooling system is composed of a water circulating chamber that is 3D printed (see Fig. 10). This chamber has small aluminum heatsinks that are glued onto the chamber. The chamber is placed between motherboard PCB and the chip-on-board PCBs since the stacking height of the SMD connectors

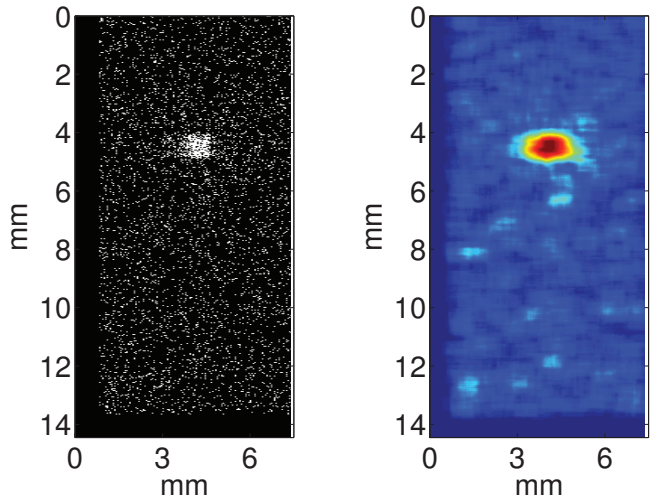

(a) (b)

Fig. 5: Signal obtained from a single scintillation event in one crystal of the 9×16 LYSO:Ce matrix of 0.8 mm pitch. (a) Raw data acquired in frame-based read out mode. (b) Processed image with 2D mean filter.

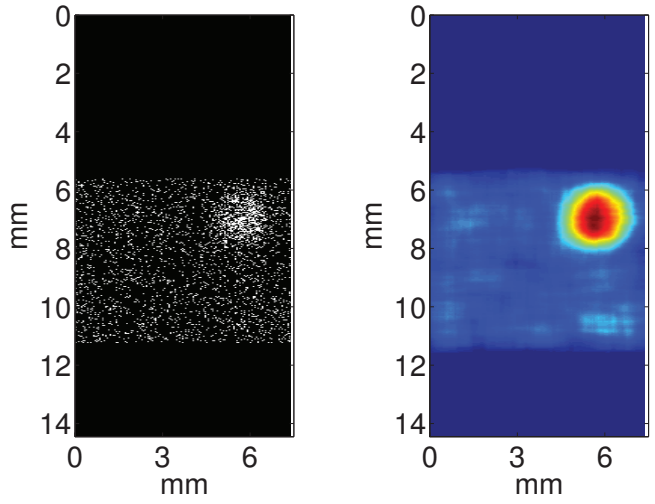

(a) (b)

Fig. 6: Signal obtained from a single scintillation event in one crystal of the 4×9 LYSO:Ce matrix of 1.6 mm pitch. (a) Raw data acquired in frame-based read out mode. (b) Processed image with 2D mean filter.

is 3 mm. The chip-on-board PCBs have square holes of 4mm side where the aluminium heatsinks are inserted. In this way, the heatsinks have direct contact with the die of the 9×18 array of MD-SiPMs.

We experimentally evaluated the cooling system performance by operating 2 chips and monitoring the temperature with and without circulating a water flow (see Fig. 11). As observed in Fig. 11 all of the chip-on-board PCBs have to be plugged in order to close the temperature sensor daisy chain. Table I shows the summary of this experiment. $I_{FPGA}+I_{2x\ dies}$ is the total current circulating in the motherboard. T_{dummy} is the

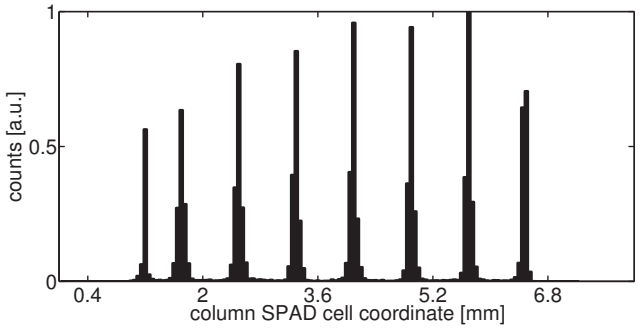

Fig. 7: 1-D histogram of the column coordinate of scintillation centroid of mass

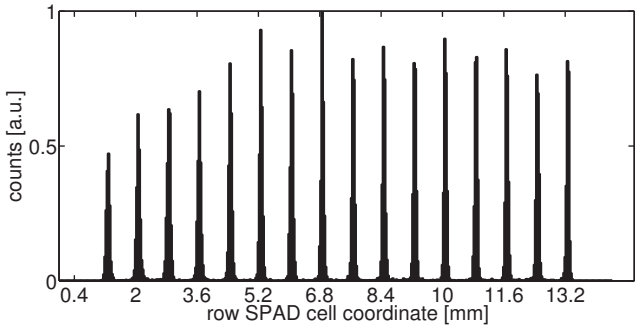

Fig. 8: 1-D histogram of the row coordinate of scintillation centroid of mass

temperature measured on the dummy PCBs that were plugged to close the temperature sensor daisy chain (see Fig. 11). And $T_{1,2}$ are the measured temperatures on the two working chip-on-board PCBs (see Fig. 11).

When there is not water flow circulating in the 3D printed chamber, the 9×18 array of MD-SiPM temperatures increases to 115 °C. However, when the water is circulating the dies are cooled down to 50 °C. This temperature allows to the proper operation of the whole MD-SiPM array chip. However, the dark count rate (DCR), which is relatively high at 50 °C, can be filtered out utilizing the DCR filtering techniques [4], [3]. We are planning to improve the cooling capabilities of the system by reducing the temperature of the circulating coolant.

VI. Current Work

In order to increase the scintillators packing fraction we designed and manufactured a 4×1 PET detector module (see Fig. 12). This module has a reduced dead space between chip-on-board PCBs. In addition, it is equipped with digital potentiometers in order to allow automatic calibrations. This detector is currently being electrically tested. After the electrical testing phase is completed, we will perform a the corresponding radiation characterization of the module.

TABLE I: Temperature characterization summary

	$I_{FPGA} + I_{2x\ dies}$ (mA)	T_{dummy}(°C)	$T_{1,2}$(°C)
Without Flow	180 + 866	60	110,115
With Flow	180 + 527	25	46,50

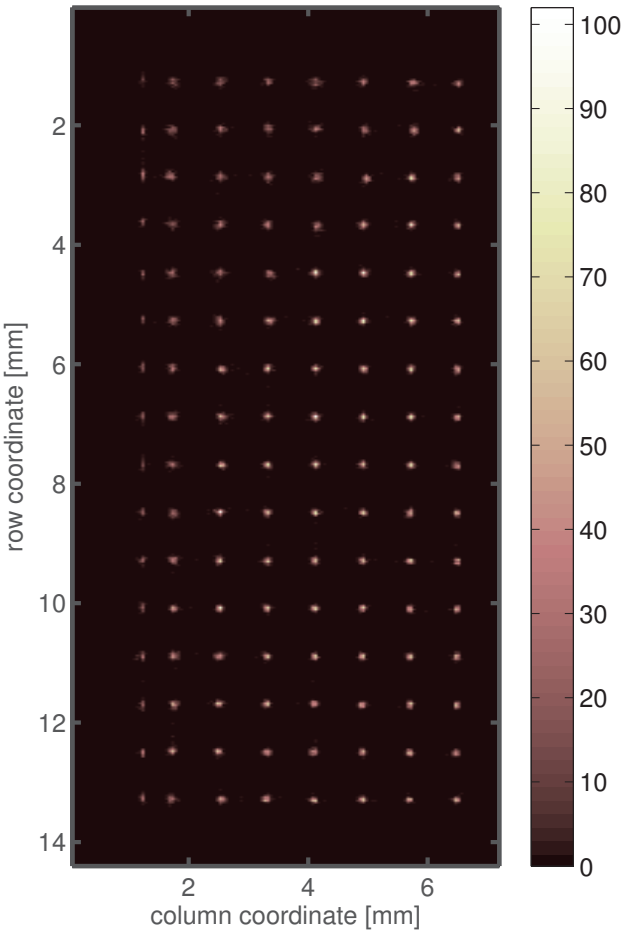

Fig. 9: 2-D histogram of the coordinates of scintillation (flood map).

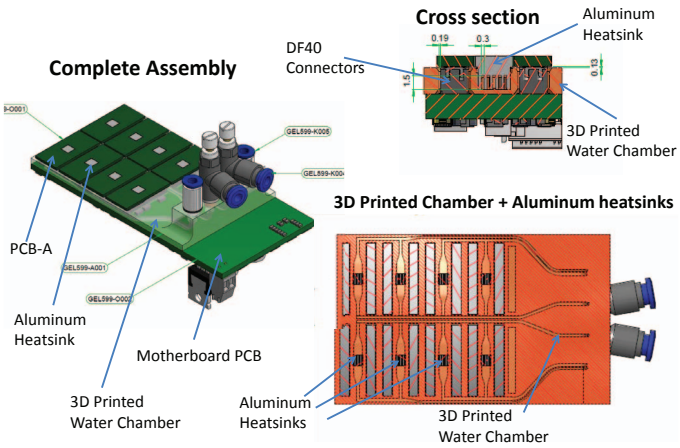

Fig. 10: Cooling system drawings

VII. Conclusions

Highly-minuaturized PET detector modules are realized. The PET detector modules have a ultra-high TDC density of $75/\mathrm{mm}^2$. These detector modules can achieve a better time resolution and DCR filtering by utilizing a multiple timestamping scheme [4], [3]. In addition, we achieved a remarkable level of miniaturization for endoscopic PET applications,

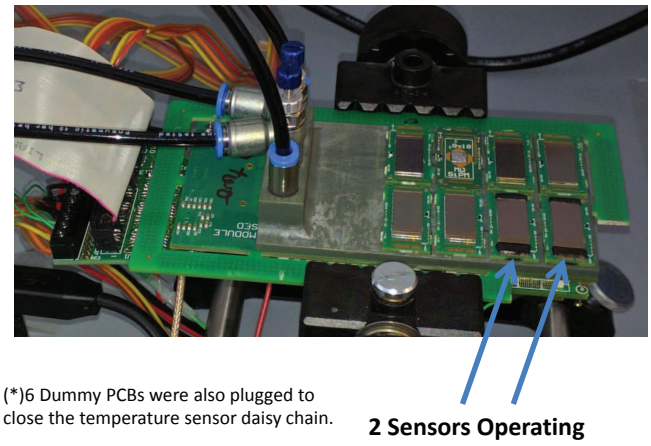

Fig. 11: Cooling system characterization

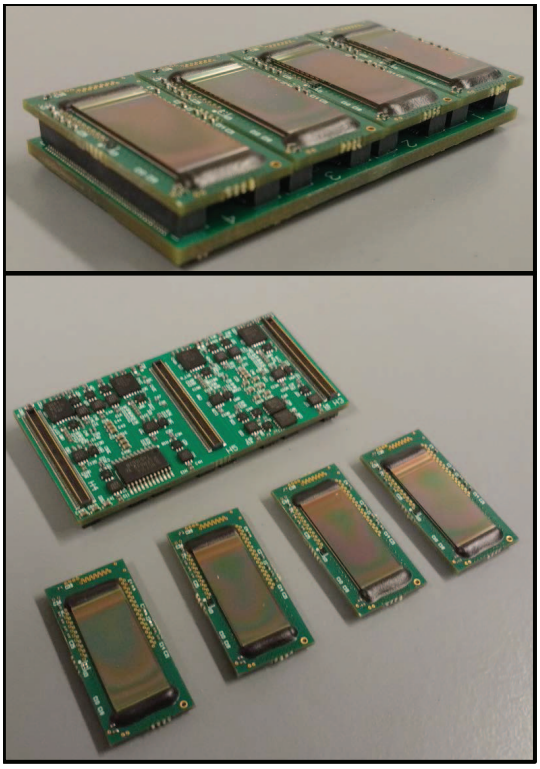

Fig. 12: 4×1 small animal PET detector module.

and in this way demonstrating the feasibility of building an endoscopic PET probe based on MD-SiPMs. Moreover, we also showed we can operate several MD-SiPMs array chips at a reasonable temperature in order to build a small-animal PET detector module. Furthermore, we showed that we can detect individual scintillations at SPAD cell level and the 0.8 mm pitch LYSO:Ce pixel identification is verified.

The boards have been designed, manufactured, and electrically tested. In addition, a preliminary radiation measurement was carried out. The current work consist of finishing the radiation characterization and testing of the 4x1 small animal PET detector module.

REFERENCES

[1] M. Fishburn and E. Charbon, "System tradeoffs in gamma-ray detection utilizing spad arrays and scintillators," *Nuclear Science, IEEE Transactions on*, vol. 57, no. 5, pp. 2549–2557, 2010.

[2] H. T. v. D. Stefan Seifert and D. R. Schaart, "The lower bound on the timing resolution of scintillation detectors," *Phys. Med. Biol.*, vol. 57, no. 7, p. 1797, 2012. [Online]. Available: http://stacks.iop.org/0031-9155/57/i=7/a=1797

[3] E. Venialgo, S. Mandai, and E. Charbon, "Time mark estimators for md-sipm and impact of system parameters," in *Nuclear Science Symposium and Medical Imaging Conference (NSS/MIC), 2013 IEEE*, Oct 2013, pp. 1–2.

[4] E. Venialgo, S. Mandai, T. Gong, D. R. Schaart, and E. Charbon, "Time estimation with multichannel digital silicon photomultipliers," *Physics in Medicine and Biology*, vol. 60, no. 6, p. 2435, 2015. [Online]. Available: http://stacks.iop.org/0031-9155/60/i=6/a=2435

[5] A. Carimatto, S. Mandai, E. Venialgo, T. Gong, G. Borghi, D. Schaart, and E. Charbon, "11.4 a 67,392-spad pvtb-compensated multi-channel digital sipm with 432 column-parallel 48ps 17b tdcs for endoscopic time-of-flight pet," in *Solid- State Circuits Conference - (ISSCC), 2015 IEEE International*, Feb 2015, pp. 1–3.

[6] S. Mandai and E. Charbon, "Multi-channel digital sipms: Concept, analysis and implementation," in *Nuclear Science Symposium and Medical Imaging Conference (NSS/MIC), 2012 IEEE*, Oct 2012, pp. 1840–1844.

[7] M. Pizzichemi, "Endotofpet-us: Towards a multi-modal endoscope for ultrasound and time of flight pet," in *2013 IEEE Nuclear Science Symposium and Medical Imaging Conference (2013 NSS/MIC)*, Oct 2013, pp. 1–5.

[8] C. Zorraquino, R. Bugalho, M. Rolo, J. C. Silva, V. Veckalns, R. Silva, C. Ortigo, J. Neves, S. Tavernier, and J. Varela, "Endotofpet-us daq, designing the data acquisition system of a high resolution endoscopic pet-us detector," in *2013 IEEE Nuclear Science Symposium and Medical Imaging Conference (2013 NSS/MIC)*, Oct 2013, pp. 1–4.

[9] E. Venialgo, S. Mandai, and E. Charbon, "Md-sipm pet detector module design," in *Nuclear Science Symposium and Medical Imaging Conference (NSS/MIC), 2014 IEEE*, November 2014, pp. 1–2.